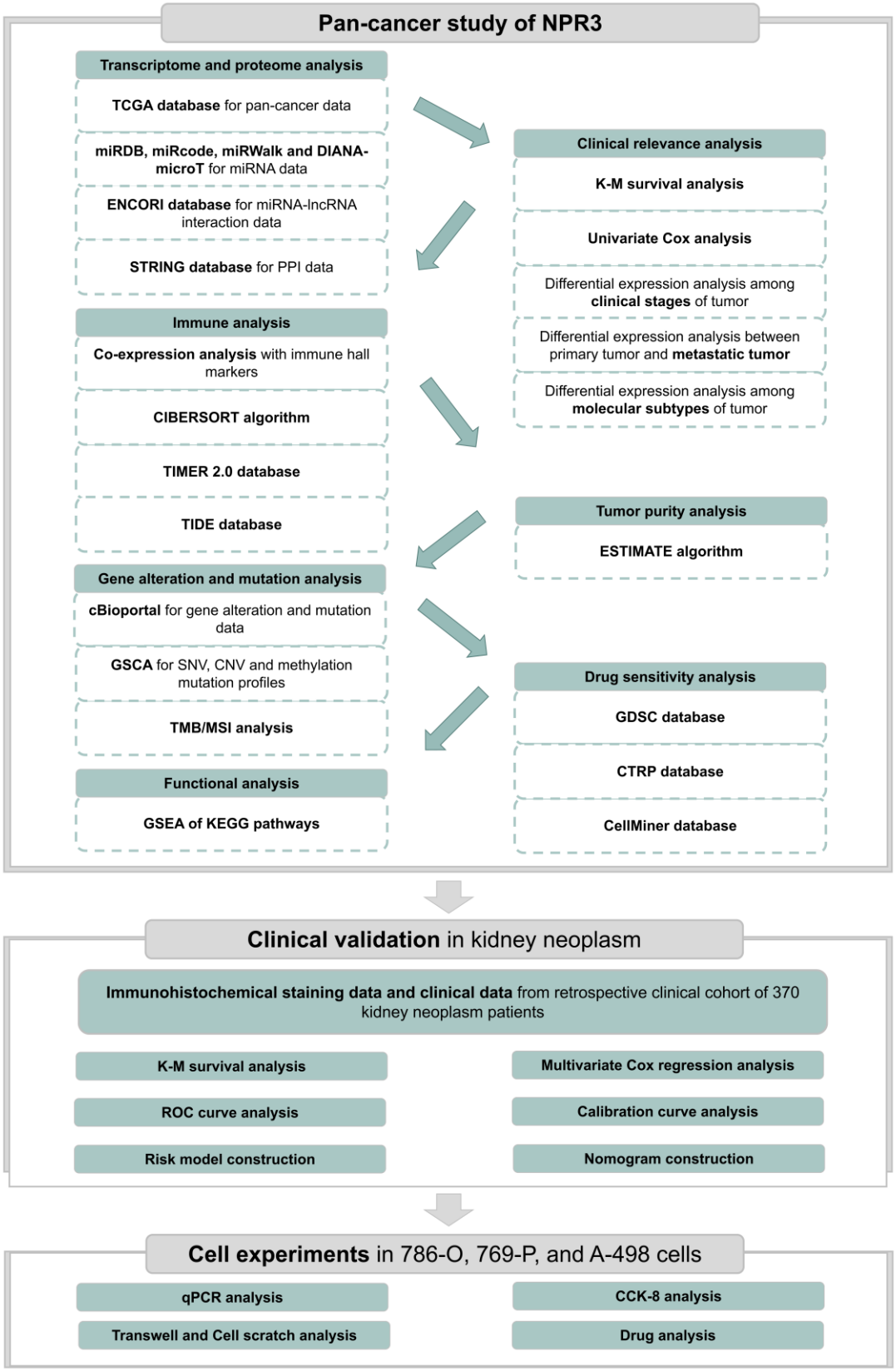

Figure S1. The flowchart of our study. *TMB, tumor mutation burden; MSI, microsatellite instability; SNV, single nucleotide variation; CNV, copy number variation; K-M, Kaplan-Meier; CCK-8, Cell counting kit-8; qPCR, quantitative real-time polymerase chain reaction.*

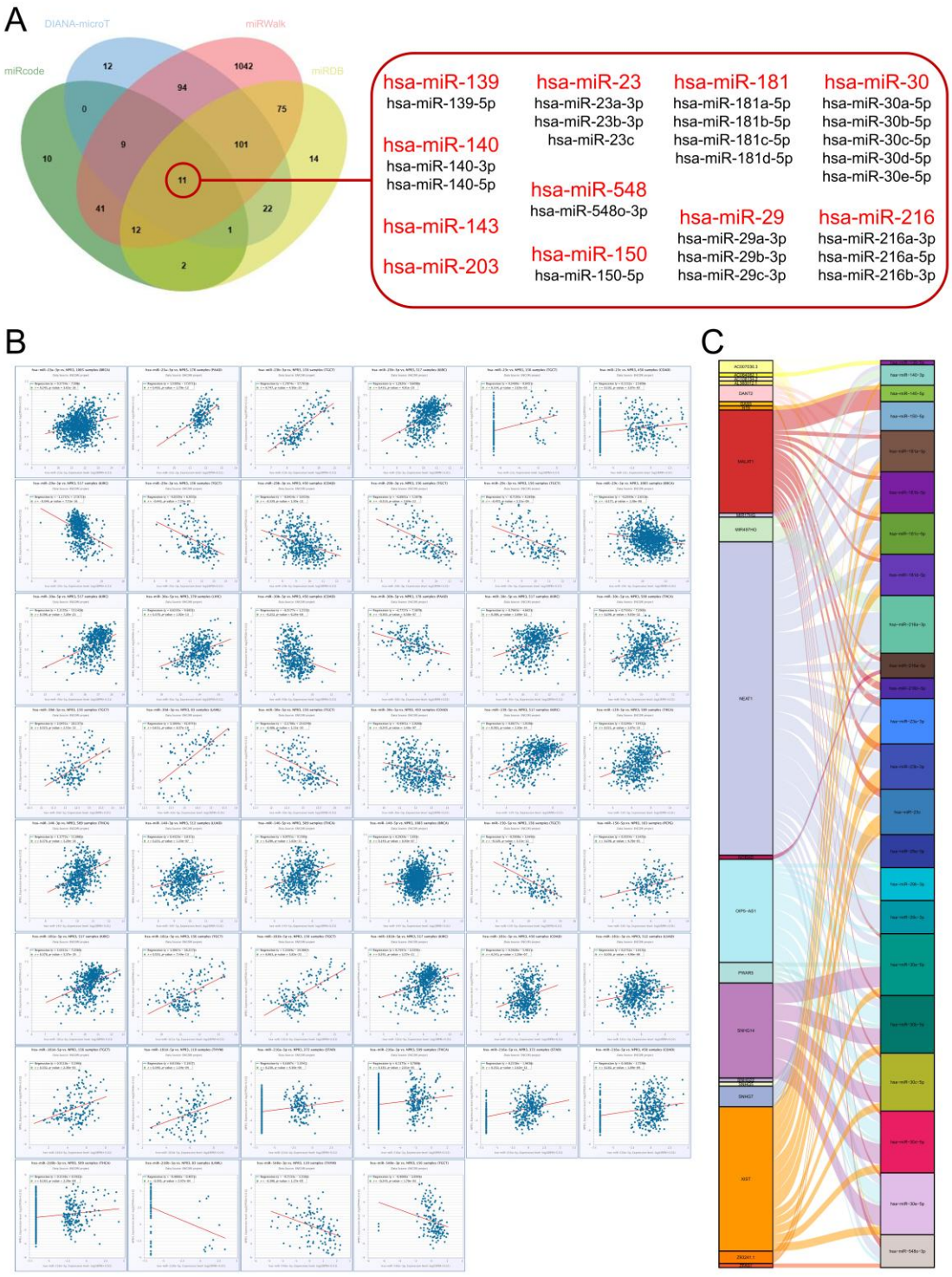

Figure S2. The construction of NPR3 ceRNA network. (**A**) The Venn diagram showed that the intersection of four miRNA databases (miRcode, Diana-microT, miRWalk and miRDB) identified 11 miRNAs, including has-miR-139, has-miR-140, has-miR-143, has-miR-203, has-miR-23, has-miR-548, has-miR-150, has-miR-181, has-miR-29, has-miR-30 and has-miR-216. (**B**) The expression level of miRNAs with NPR3 expression in pan-cancer. The results were significant in various cancer types, especially in KIRC, TGCT, COAD, THCA, etc. (**C**) The Sanky diagram showed the interaction between miRNA and lncRNA. The 23 miRNAs included hsa-miR-139-5p, hsa-miR-140-3p, hsa-miR-140-5p, hsa-miR-150-5p, hsa-miR-181a-5p, hsa-miR-181b-5p, hsa-miR-181c-5p, hsa-miR-181d-5p, hsa-miR-

548o-3p, hsa-miR-216a-3p, hsa-miR-216a-5p, hsa-miR-216b-5p, hsa-miR-23a-3p, hsa-miR-23b-3p, hsa-miR-23c, hsa-miR-29a-3p, hsa-miR-29b-3p, hsa-miR-29c-3p, hsa-miR-30a-5p, hsa-miR-30b-5p, hsa-miR-30c-5p, hsa-miR-30d-5p and hsa-miR-30e-5p. The 21 lncRNAs included AC084082.1, NEAT1, MIR17HG, MIR497HG, XIST, H19, MALAT1, SNHG7, DANT2, GAS5, OIP5-AS1, ZFAS1, SNHG22, SNHG5, AC108134.2, NORAD, AL360012.1, Z93241.1, AC007036.3, SNHG14 and PWAR5.

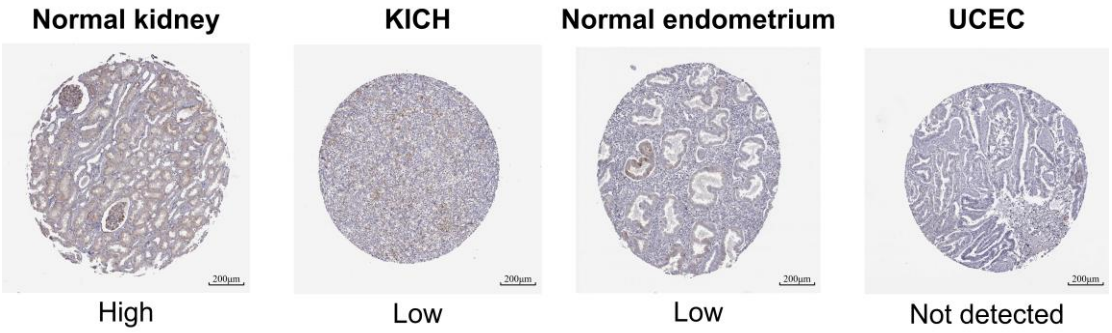

Figure S3. IHC pictures of NPR3 from HPA database. Representative IHC images showed that NPR3 expressed less in tumor tissues than in normal kidney and endometrium. *IHC, Immunohistochemical.*

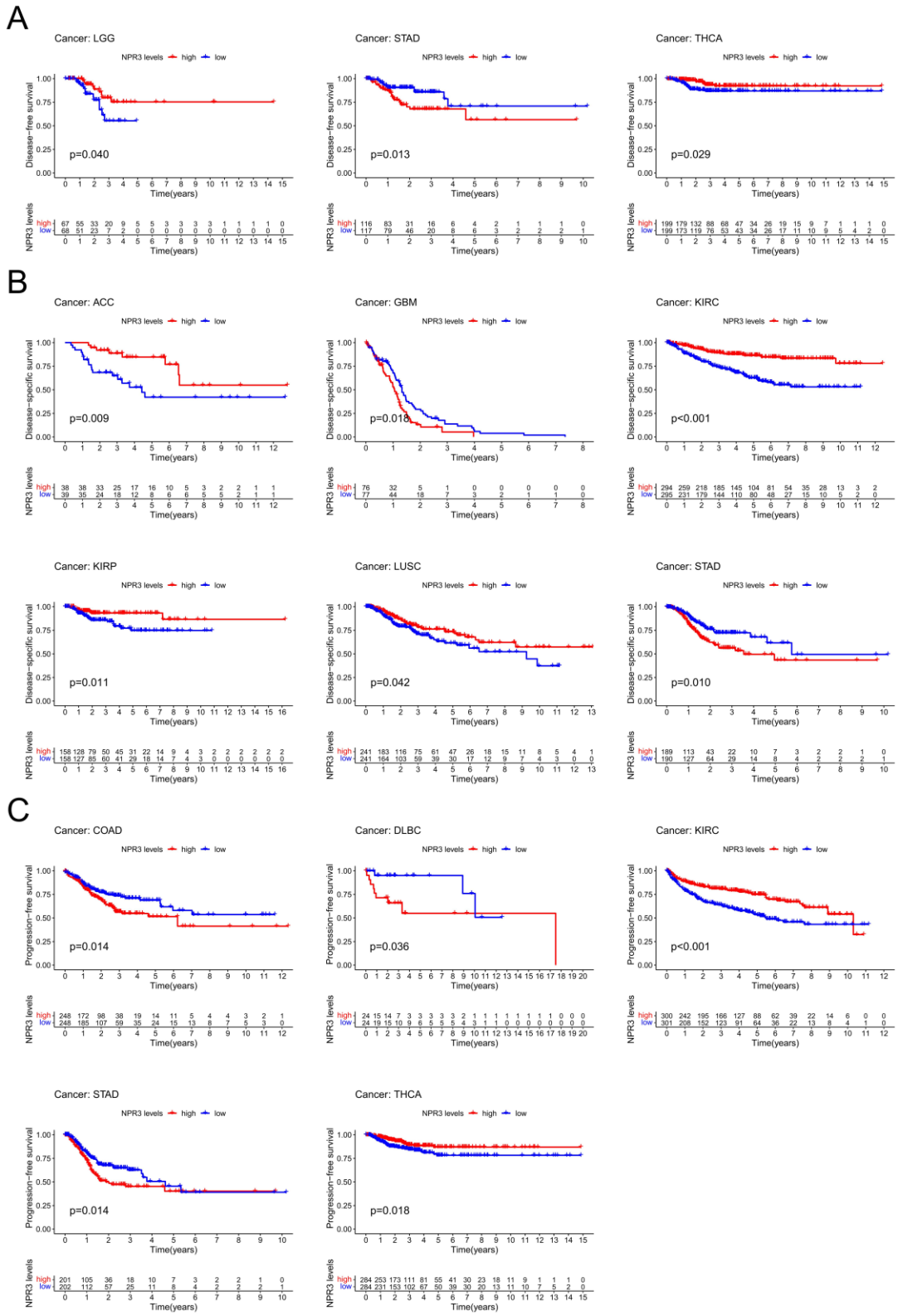

Figure S4. Survival analysis between low- and high-NPR3 expression groups in DFS, DSS and PFS. Only cancer types which were statistically significant differences were shown. (**A**) NPR3 was positively correlated with DFS in LGG (p = 0.04) and THCA (p = 0.029), while it was negatively correlated in STAD (p = 0.013). (**B**) NPR3 was positively correlated with DSS in ACC (p = 0.009), KIRC (p < 0.001), KIRP (p = 0.011) and LUSC (p = 0.042), whereas it was negatively correlated in GBM (p = 0.018) and

STAD (p = 0.01). (**C**) NPR3 was positively correlated with PFS in KIRC (p < 0.001) and THCA (p = 0.018), while it was negatively correlated in COAD (p = 0.014), DLBC (p = 0.036) and STAD (p = 0.014). *DFS, Disease-free survival; DSS, Disease-specific survival; PFS, Progression-free survival.*

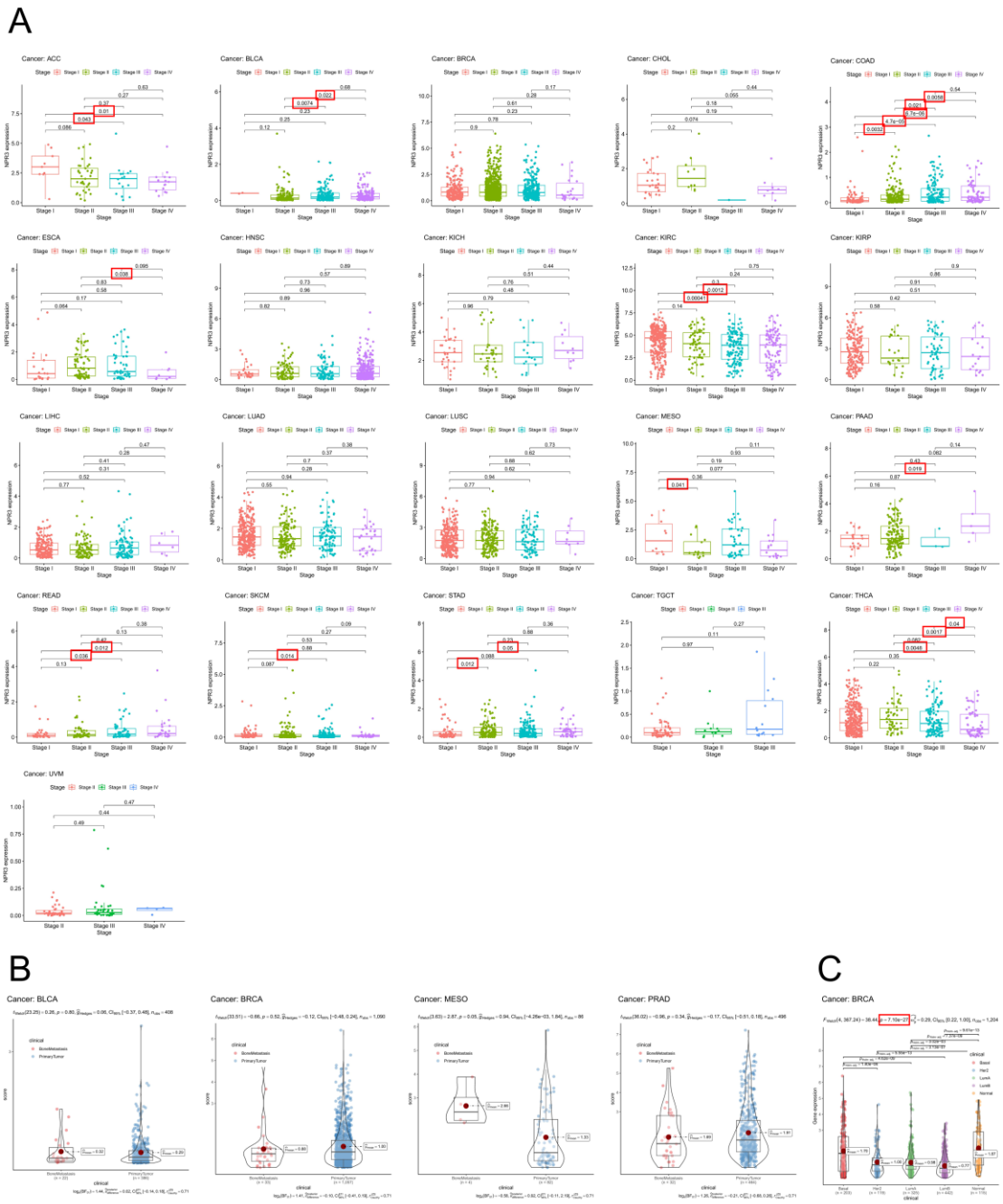

Figure S5. Clinical relevance analysis in clinical stages, bone metastasis and molecular subtypes. (**A**) Clinical relevance analysis in clinical stages. NPR3 was positively correlated with the clinical stage of COAD and READ, while it was negatively correlated in KIRC. (**B**) Bone metastasis analysis. The expression of NPR3 was not significantly different in primary tumor and metastatic ones in BLCA, BRCA, MESO and PRAD. (**C**) Molecular subtype analysis. The expression level of NPR3 was statistically different among various molecular subtypes of BRCA.

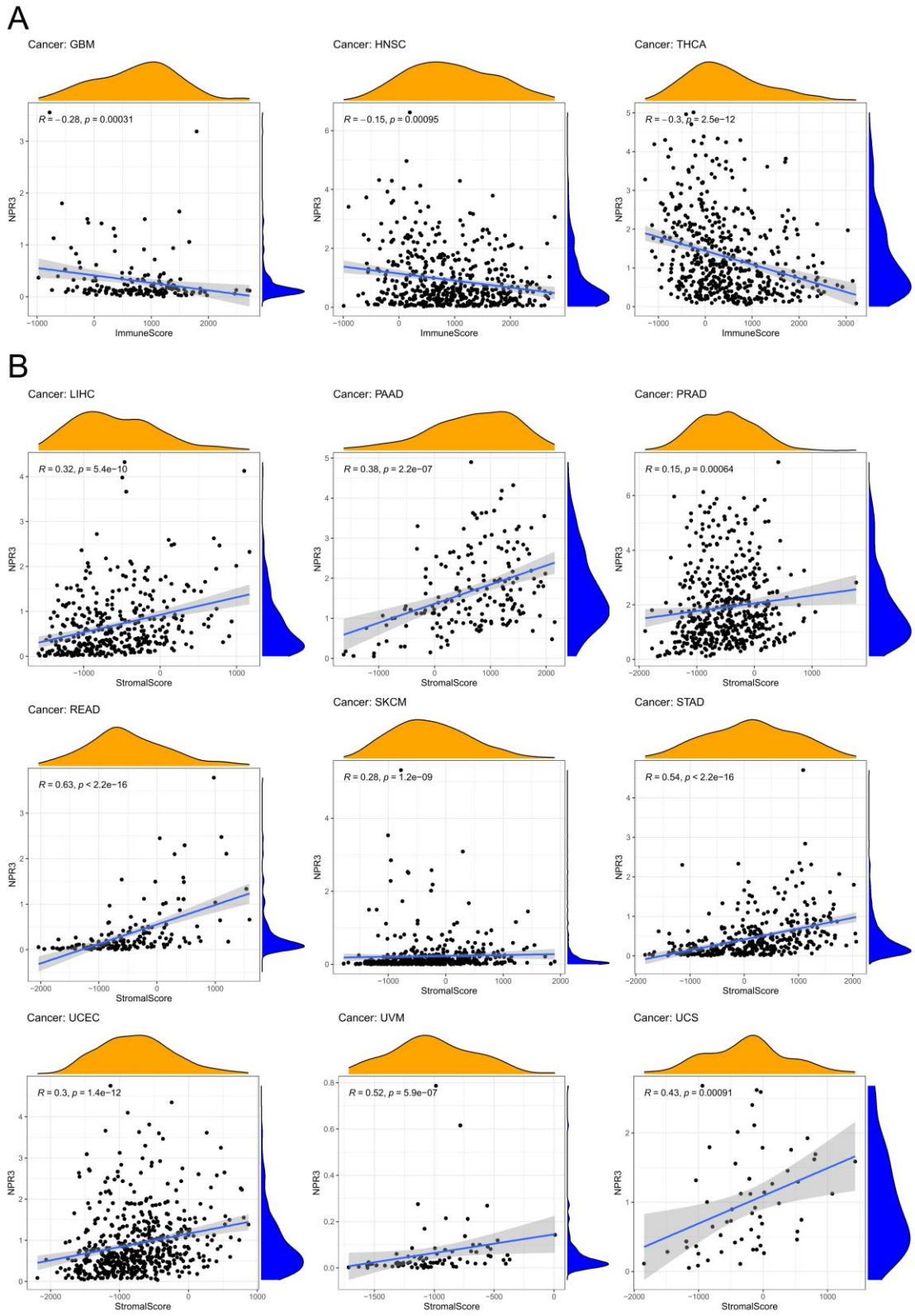

Figure S6. Relationship of NPR3 expression with TME and TMB in pan-cancer. (**A**) Correlation of NPR3 expression with immune scores. It was negatively correlated in GBM (R = -0.28, $p < 0.001$), HNSC (R = -0.15, $p < 0.001$), and THCA (R = -0.3, $p < 0.001$). (**B**) Correlation of NPR3 expression with stromal scores. It was positively correlated with stromal scores in LIHC (R = 0.32, $p < 0.001$), PAAD (R = 0.38, $p < 0.001$), PRAD (R = 0.15, $p < 0.001$), READ (R = 0.63, $p < 0.001$), SKCM (R =

0.28, $p < 0.001$), STAD (R = 0.54, $p < 0.001$), UCEC (R = 0.3, $p < 0.001$), UVM (R = 0.52, $p < 0.001$), and UCS (R = 0.43, $p < 0.001$). *TME, Tumor microenvironment; TMB, Tumor mutation burden.*

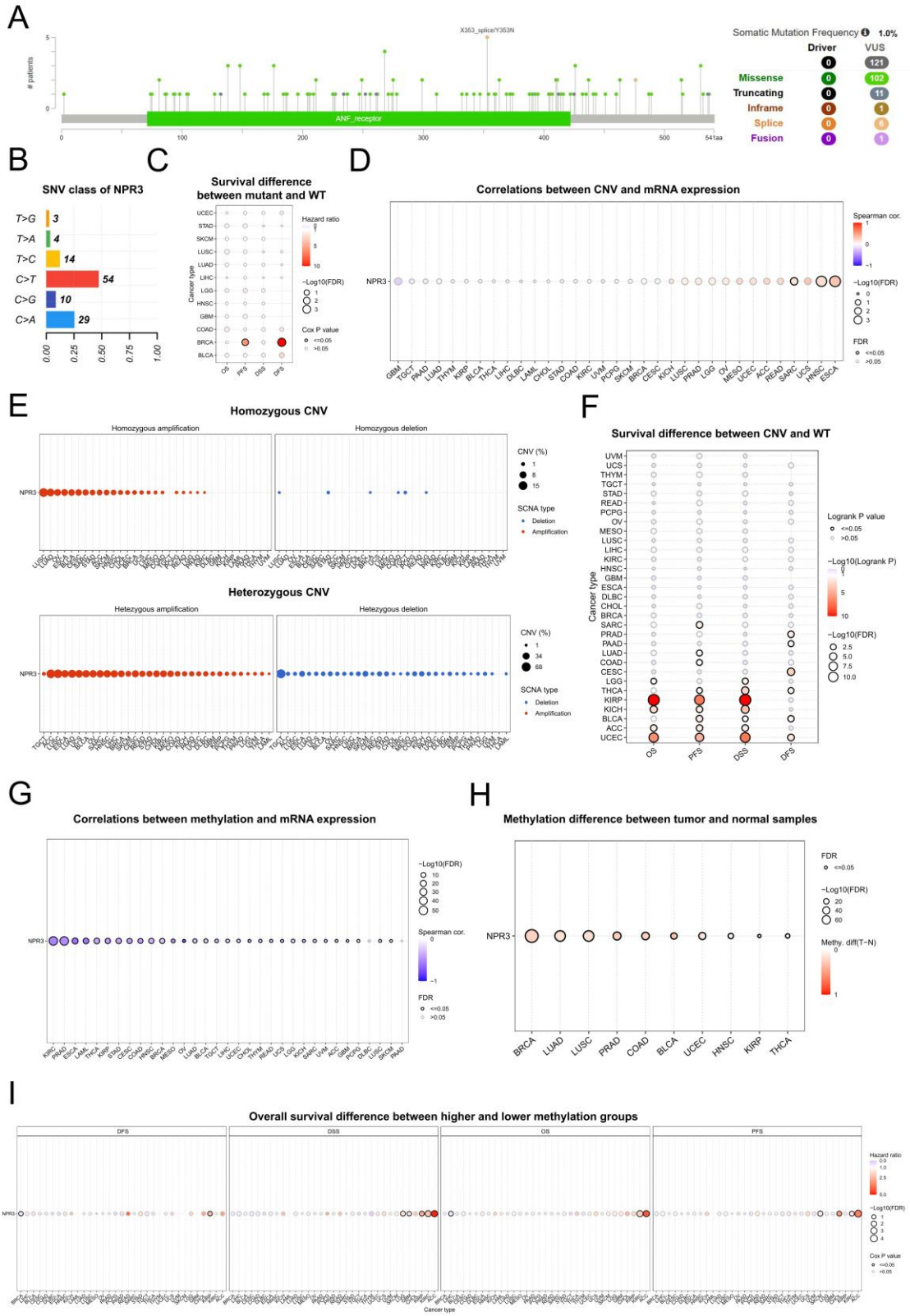

Figure S7. Gene alteration and mutation analysis of NPR3. (**A**) From cBioportal, gene alteration types and frequencies in pan-cancer were recognized. (**B**) SNV classes of NPR3. C to T variation was the most common in NPR3. (**C**) Survival difference between mutant and wild type. The mutant was a significant

risk factor in BRCA (PFS and DFI). (**D**) Correlations between CNV and mRNA expression. CNV was positively correlated with mRNA expression in SARC, HNSC, and ESCA. (**E**) The profile of homozygous/heterozygous CNV. (**F**) Survival difference between CNV and wide type. The CNV was a significant risk factor in KIRP, KICH, UCEC, BLCA, ACC, etc. (**G**) Correlations between methylation and mRNA expression. The methylation was negatively correlated with mRNA expression in all tumor types except DLBC and PAAD. (**H**) Methylation difference between tumor and normal samples. Methylation was significantly up-regulated in tumor tissues in BRCA, LUAD, LUSC, PRAD, COAD, BLCA, UCEC, HNSC, KIRP and THCA (**I**) The overall survival difference between higher and lower methylation groups. Methylation was a protective factor of DFI in BRCA, of OS in LIHC. However, it was a risk factor of PFI in KIRP, of DSS in LGG, GBM, KIRP, KIRC and ACC, of OS in KIRC and ACC, of PFS in SKCM, CHOL, KIRC and ACC. *SNV, Single nucleotide variation; WT, Wild type.; CNV, Copy number variation; OS, Overall survival; DFS, Disease-free survival; DSS, Disease-specific survival; PFS, Progression-free survival.*

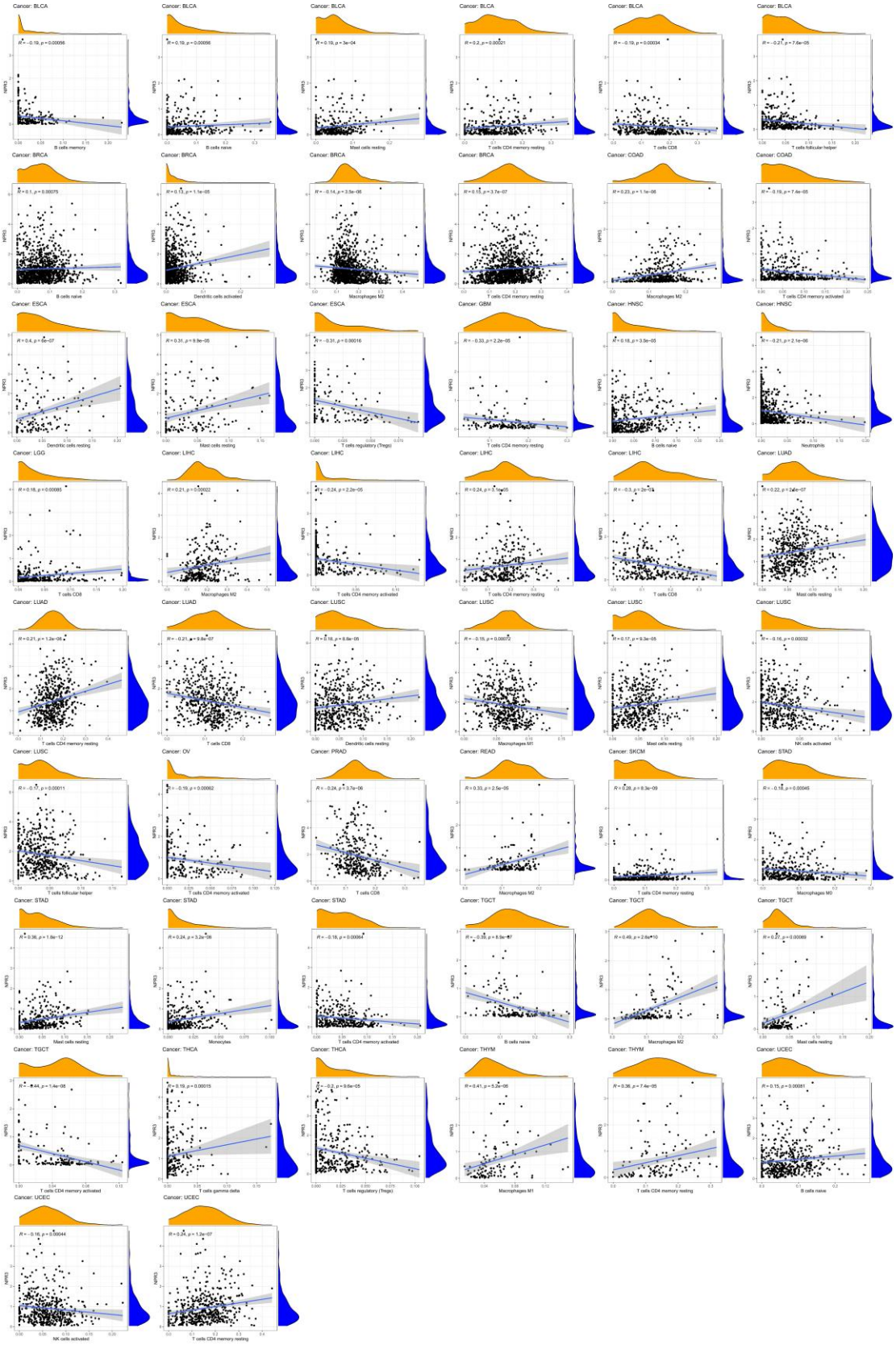

Figure S8. ESTIMATE analysis of correlation between NPR3 expression and immune cell infiltration in pan-cancer. In BLCA, NPR3 expression was negatively correlated with B cells memory, mast cells, T cells CD8 and T cells follicular helper resting, while it was positively correlated with B cells naïve, T cells CD4 memory resting. In BRCA, NPR3 expression was positively correlated with B cells naïve,

dendritic cells activated and T cells CD4 memory resting, while it was negatively correlated with macrophages M2. In COAD, NPR3 expression was positively correlated with macrophages M2, while it was negatively correlated with T cells CD4 memory activated. In ESCA, NPR3 expression was positively correlated with dendritic cells resting, mast cells resting, while it was negatively correlated with Tregs. In GBM, NPR3 expression was negatively correlated with T cells CD4 memory resting. In HNSC, NPR3 expression was positively correlated with B cells naïve, while it was negatively correlated with neutrophils. In LGG, NPR3 expression was positively correlated with T cells CD8. In LIHC, NPR3 expression was positively correlated with macrophages M2 and T cells CD4 memory resting, while it was negatively correlated with T cells CD4 memory activated and T cells CD8. In LUAD, NPR3 expression was positively correlated with mast cells resting and T cells CD4 memory resting, while it was negatively correlated with T cells CD8. In LUSC, NPR3 expression was correlated with dendritic cells resting and mast cells resting, while it was negatively correlated with macrophages M1, NK cells activated and T cells follicular helper. In OV, NPR3 expression was negatively correlated with T cells CD4 memory activated. In PRAD, NPR3 expression was negatively correlated with T cells CD8. In READ, NPR3 expression was positively correlated with macrophages M2. In SKCM, NPR3 expression was positively correlated with T cells CD4 memory resting. In STAD, NPR3 expression was negatively correlated with macrophages M0 and T cells CD4 memory activated, while it was positively correlated with mast cells resting and monocytes. In TGCT, NPR3 expression was negatively correlated with B cells naïve and T cells CD4 memory activated, while it was positively correlated with macrophages M2 and mast cells resting. In THCA, NPR3 expression was positively correlated with T cells gamma delta, while it was negatively correlated with Tregs. In THYM, NPR3 expression was positively correlated with macrophages M1 and T cells CD4 memory resting. In UCEC, NPR3 expression was positively correlated with B cells naïve and T cells CD4 memory resting, while it was negatively correlated with NK cells activated. *Tregs, T cells regulatory.*

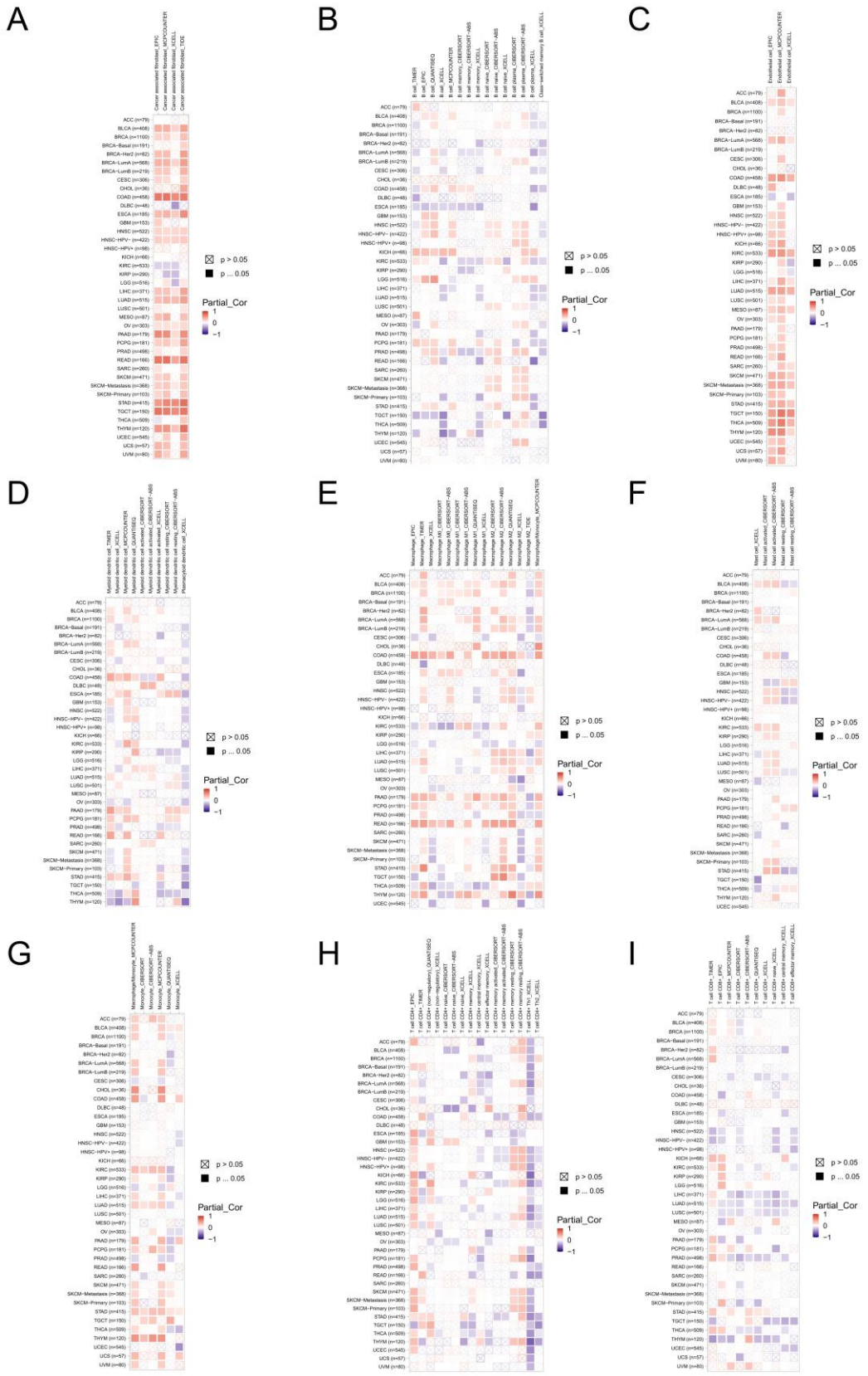

Figure S9. TIMER 2.0 database analysis of correlation between NPR3 expression and immune cell infiltration in pan-cancer. (**A**) NPR3 expression was positively correlated with cancer-associated fibroblasts in all cancer types except DLBC, KIRC and KIRP. (**B**) NPR3 expression was negatively correlated with B cells in BRCA, CESC, ESCA and KIRC, while it was positively corelated in GBM,

HNSC, KICH, SKCM and UCEC. (**C**) NPR3 expression was positively correlated with endothelial cells in all cancer types except ESCA. (**D**) NPR3 expression was positively correlated with myeloid dendritic cells in COAD, ESCA, PAAD, PCPG and SARC, while it was negatively corelated in KIRP, THCA and THYM. (**E**) NPR3 expression was positively correlated with macrophages in BLCA, BRCA, COAD, PRAD, PCPG, READ and THYM, while it was negatively corelated in CESC, KIRC and THCA. (**F**) NPR3 expression was positively correlated with mast cells in BRCA, KIRC, KIRP and PCPG. (**G**) NPR3 expression was positively correlated with monocytes in ACC, BLCA, COAD, KIRC, LUAD, SKCM, STAD, THYM and UCS, while it was negatively corelated in PRAD. (**H**) NPR3 expression was negatively correlated with $CD4^+$ T cells in BRCA, COAD and KIRC, while it was positively corelated in SKCM. (**I**) NPR3 expression was negatively correlated with $CD8^+$ T cells in CESC, HNSC, LIHC, LUAD, LUSC, PRAD, TGCT and THYM.

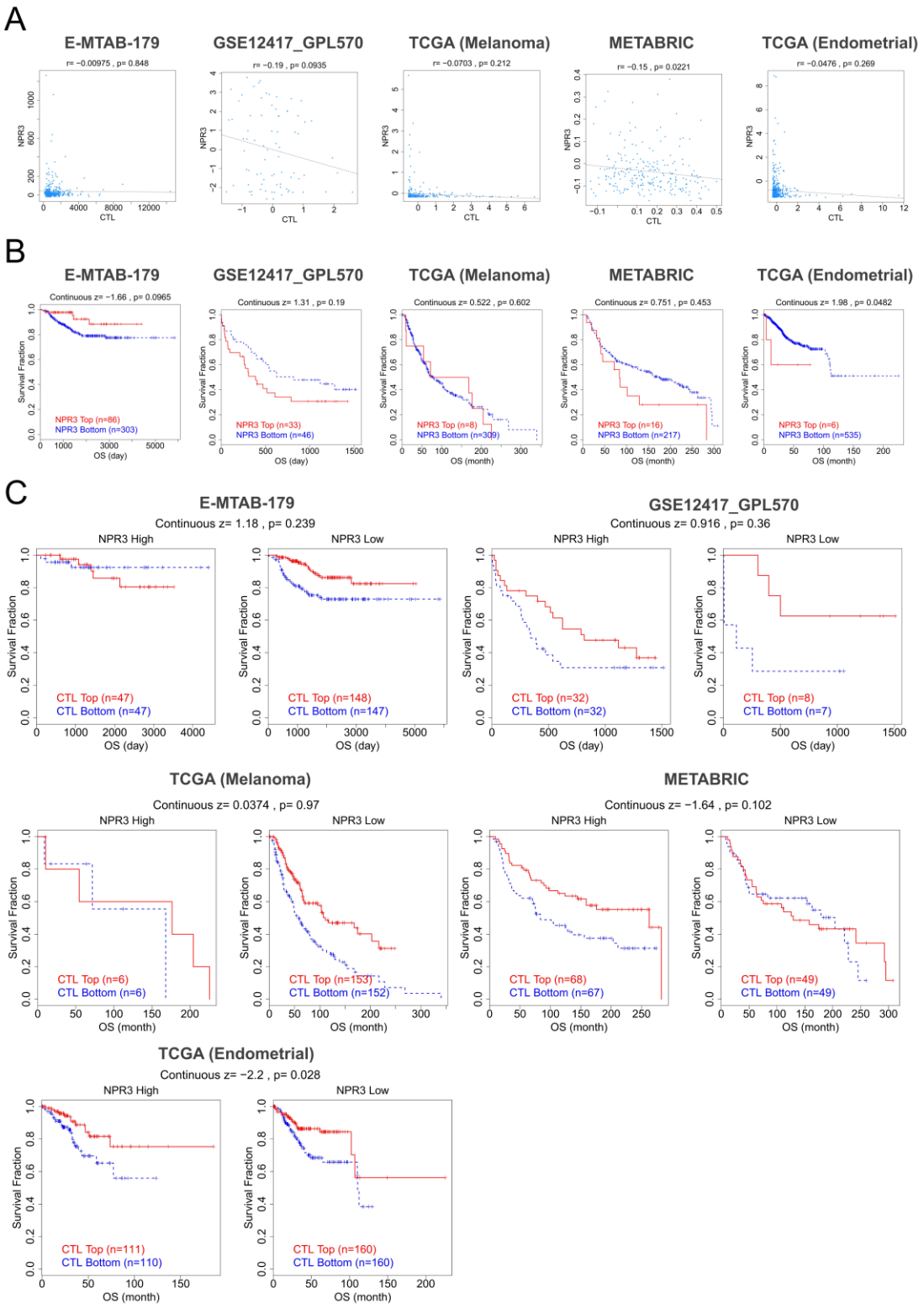

Figure S10. TIDE database analysis of correlation between NPR3 expression and cytotoxic T lymphocyte (CTL) in pan-cancer. (**A**) NPR3 expression was negatively correlated with CTL in BRCA (r = -0.15, p = 0.022). (**B**) Lower NPR3 expression was correlated with better survival in UCEC (z = 1.98, p = 0.048). (**C**) Cox proportional hazards model indicated that NPR3 expression was negatively correlated with CTL in UCEC (z = -2.2, p = 0.028).

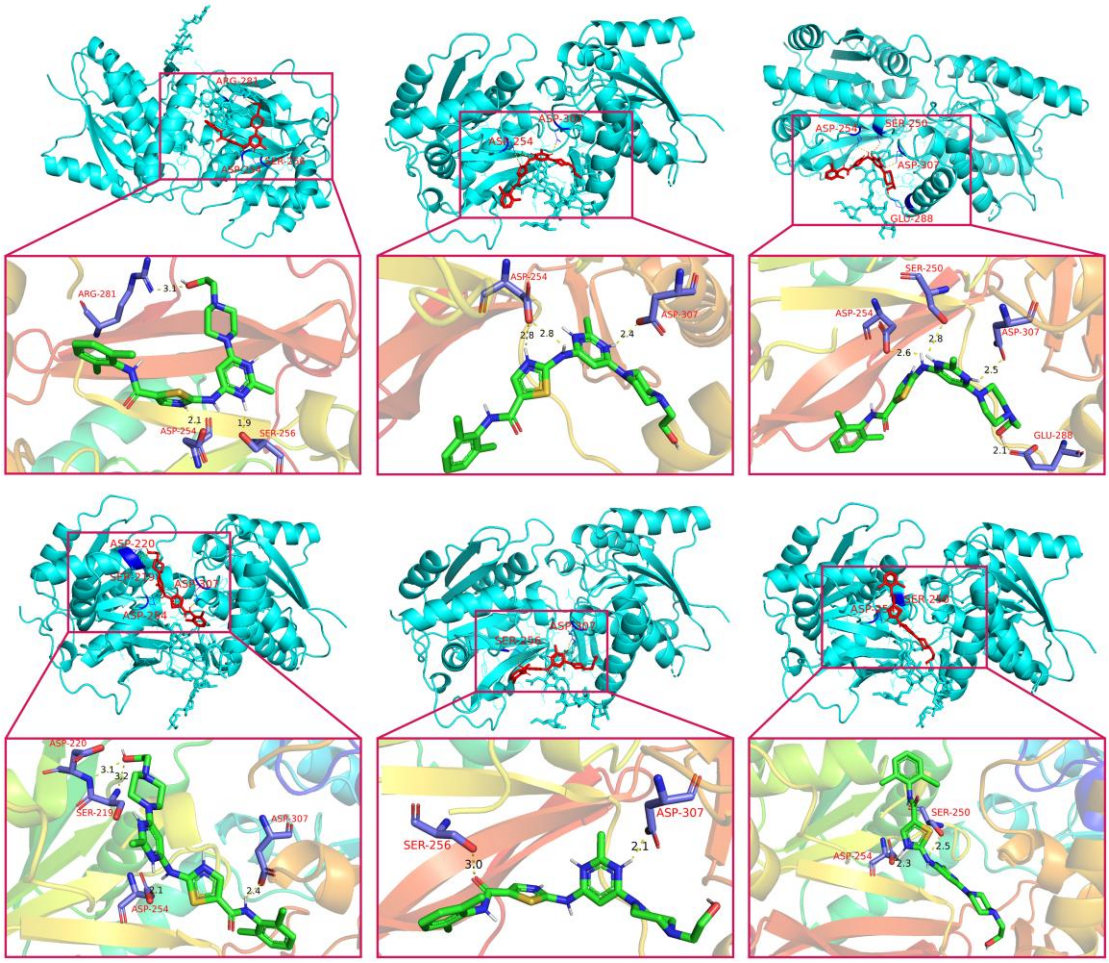

Figure S11. Possible binding sites between NPR3 and dasatinib.

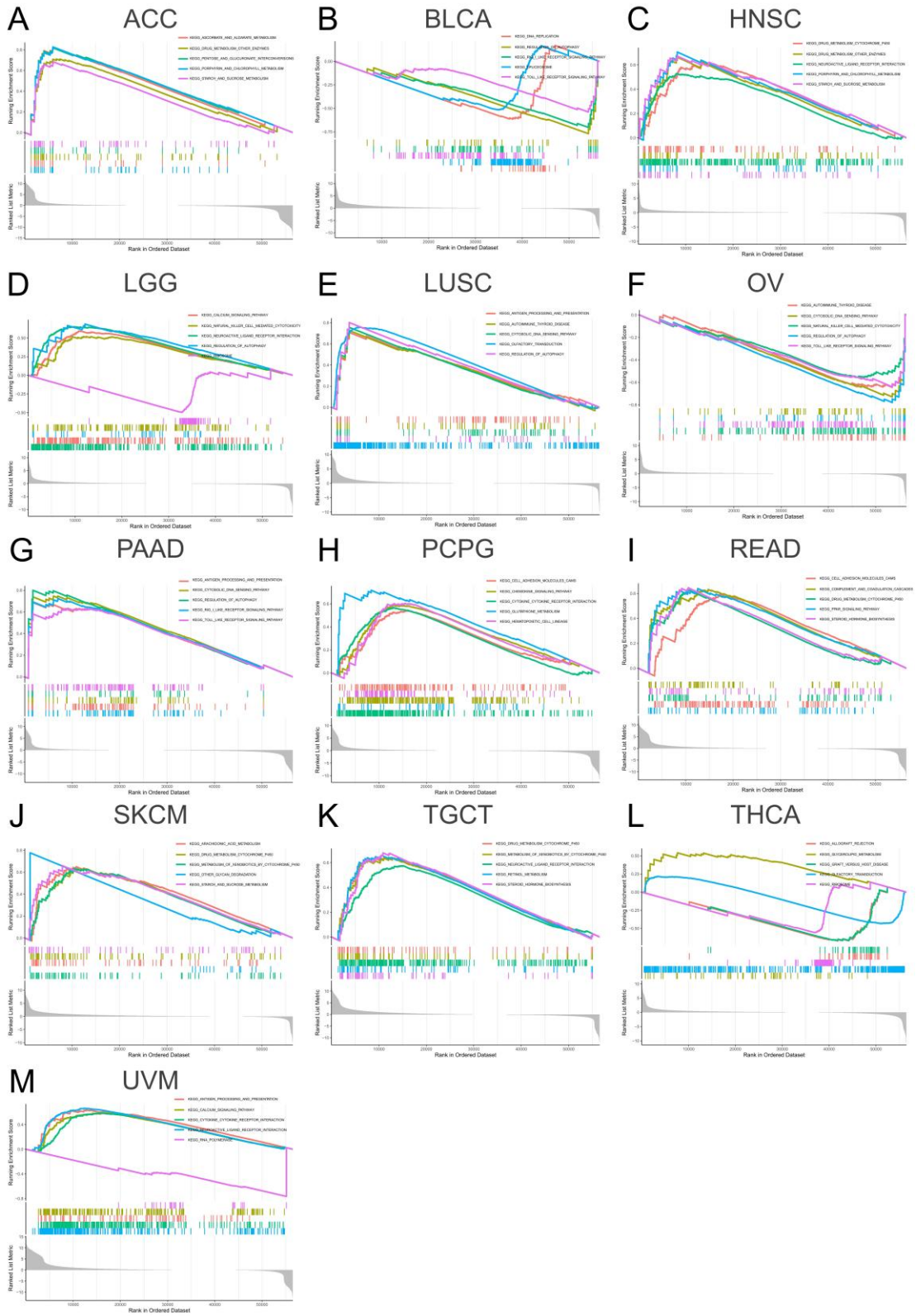

Figure S12. GSEA analysis of NPR3 in pan-cancer. (**A**) In ACC, the top five KRGG pathways were "ascorbate and aldarate metabolism", "drug metabolism - other enzymes", "pentose and glucuronate interconversions", "porphyrin and chlorophyll metabolism" and "starch and sucrose metabolism". (**B**) In BLCA, the top five KRGG pathways were "DNA replication", "regulation of autophagy", "RIG-I-like receptor signaling pathway", "spliceosome" and "Toll-like receptor signaling pathway". (**C**) In HNSC,

the top five KRGG pathways were “drug metabolism - cytochrome P450”, “drug metabolism - other enzymes”, “neuroactive ligand receptor interaction”, “porphyrin and chlorophyll metabolism”, and “starch and sucrose metabolism”. (**D**) In LGG, the top five KRGG pathways were “calcium signaling pathway”, “natural killer cell mediated cytotoxicity”,“neuroactive ligand receptor interaction”, “regulation of autophagy” and “ribosome”. (**E**) In LUSC, the top five KRGG pathways were “antigen processing and presentation”, “autoimmune thyroid disease”, “cytosolic DNA sensing pathway”, “olfactory transduction” and “regulation of autophagy”. (**F**) In OV, the top five KRGG pathways were “autoimmune thyroid disease”, “cytosolic DNA sensing pathway”, “natural killer cell mediated cytotoxicity”, “regulation of autophagy” and “Toll-like receptor signaling pathway”. (**G**) In PAAD, the top five KRGG pathways were “antigen processing and presentation”, “cytosolic DNA sensing pathway”, “regulation of autophagy”, “RIG-I-like receptor signaling pathway” and “Toll-like receptor signaling pathway”. (**H**) In PCPG, the top five KRGG pathways were “cell adhesion molecules CAMs”, “chemokine signaling pathway”, “cytokine – cytokine receptor interaction”, “glutathione metabolism” and “hematopoietic cell lineage”. (**I**) In READ, the top five KRGG pathways were “cell adhesion molecules CAMs”, “complement and coagulation cascades”, “drug metabolism – cytochrome P450”, “PPAR signaling pathway” and “steroid hormone biosynthesis”. (**J**) In SKCM, the top five KRGG pathways were “arachidonic acid metabolism”, “drug metabolism – cytochrome P450”, “metabolism of xenobiotics by cytochrome P450”, “other glycan degradation” and “starch and sucrose metabolism”. (**K**) In TGCT, the top five KRGG pathways were “drug metabolism – cytochrome P450”, “metabolism of xenobiotics by cytochrome P450”, “neuroactive ligand receptor interaction”, “retinol metabolism” and “steroid hormone biosynthesis”. (**L**) In TGCT, the top five KRGG pathways were “allograft rejection”, “glycerolipid metabolism”, “graft versus host disease”, “olfactory transduction” and “ribosome”.

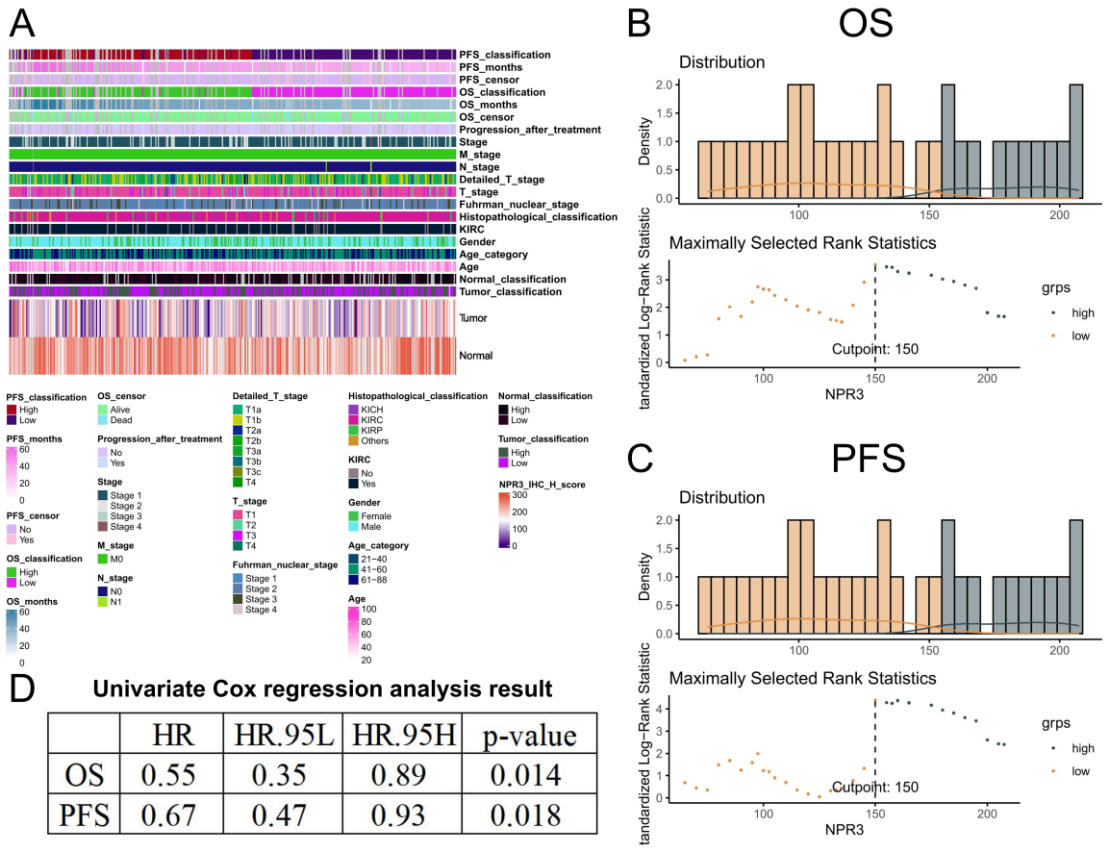

D **Univariate Cox regression analysis result**

	HR	HR.95L	HR.95H	p-value
OS	0.55	0.35	0.89	0.014
PFS	0.67	0.47	0.93	0.018

Figure S13. The cutoff point of IHC scores and the heatmap with Chi square analysis. (**A**) The heatmap summarizing the demographic and clinicopathological features of the cohort, which included 370 kidney neoplasm patients. (**B**) The cutoff point of IHC scores of NPR3 in kidney neoplasm was 150 in OS. (**C**) The cutoff point of IHC scores of NPR3 in kidney neoplasm was 150 in PFS. (**D**) The table showing the result of univariate Cox regression analysis. NPR3 expression was protective factor for OS (HR = 0.55, 95%CI = 0.35 - 0.89, $p = 0.014$) and PFS (HR = 0.67, 95%CI = 0.47 - 0.93, $p = 0.018$). *IHC, Immunohistochemical; OS, Overall survival; PFS, Progression-free survival. *p < 0.05, **p < 0.01, ***p < 0.001.*

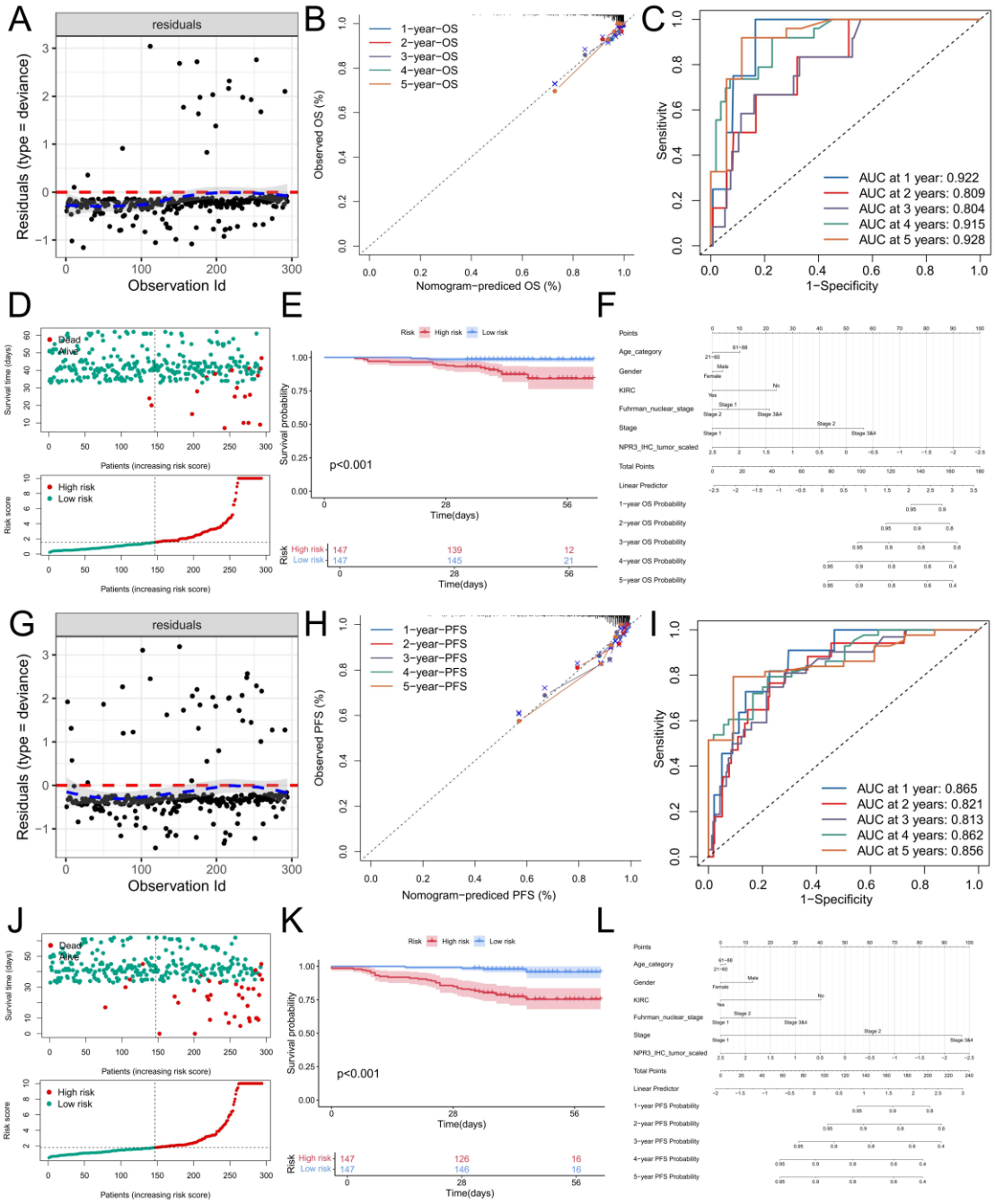

Figure S14. Model diagnosis and nomogram construction for OS and PFS.

(**A**) The deviance residual plot showed that the residuals were randomly scattered about zero with no clear pattern. (**B**) The calibration curves showed that the predicted 1-, 2-, 3-, 4-, and 5-year-OS closely

matched with the actual outcomes. (**C**) The ROC curves provided the AUC at 1 year (0.922), 2 years (0.809), 3 years (0.804), 4 years (0.915), and 5 years (0.928). (**D**) A risk model was constructed, and all samples were split into high- and low-risk groups according to the median risk score. (**E**) The K-M survival curve demonstrated that patients with higher risk scores had significantly poorer OS ($p < 0.001$). (**F**) A nomogram was constructed for predicting 1-, 2-, 3-, 4-, and 5-year OS probability for kidney neoplasm patients. (**G**) The deviance residual plot showed that the residuals were randomly scattered about zero with no clear pattern. (**H**) The calibration curves showed that the predicted 1-, 2-, 3-, 4-, and 5-year-PFS closely matched with the actual outcomes. (**I**) The ROC curves provided the AUC at 1 year (0.865), 2 years (0.821), 3 years (0.813), 4 years (0.862), and 5 years (0.856). (**J**) A risk model was constructed, and all samples were split into high- and low-risk groups according to the median risk score. (**K**) The K-M survival curve demonstrated that patients with higher risk scores had significantly poorer OS ($p < 0.001$). (**L**) A nomogram was constructed for predicting 1-, 2-, 3-, 4-, and 5-year PFS probability for kidney neoplasm patients. *OS, Overall Survival; PFS, Progression-Free Survival; K-M, Kaplan-Meier; OS, Overall Survival; HR, Hazard Ratio; CI, Confidence Interval; ROC, Receiver Operating Characteristic, AUC, Area Under Curve.*

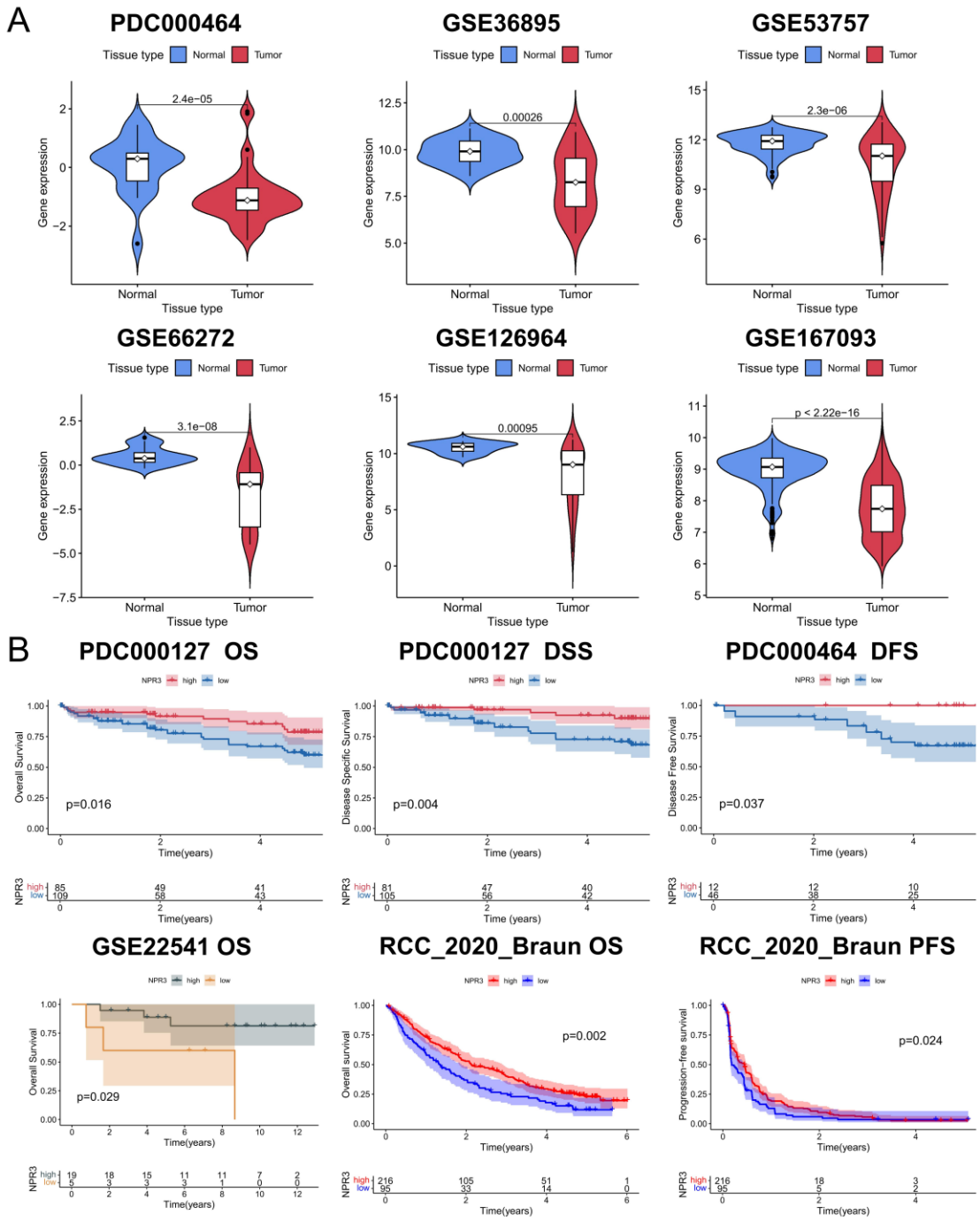

Figure S15. External validation of NPR3 expression. (**A**) The differential expression analysis confirmed that NPR3 expression was significantly down-regulated in kidney neoplasms ($p < 0.001$) compared to normal tissues, which aligns with our findings. (**B**) K-M survival curves showed that higher NPR3 expression was significantly associated with better survival outcomes ($p < 0.05$) in kidney neoplasm patients, further supporting our results. *K-M, Kaplan-Meier; OS, Overall Survival; DFS, Disease-Free Survival; DSS, Disease-Specific Survival; PFS, Progression-Free Survival.*

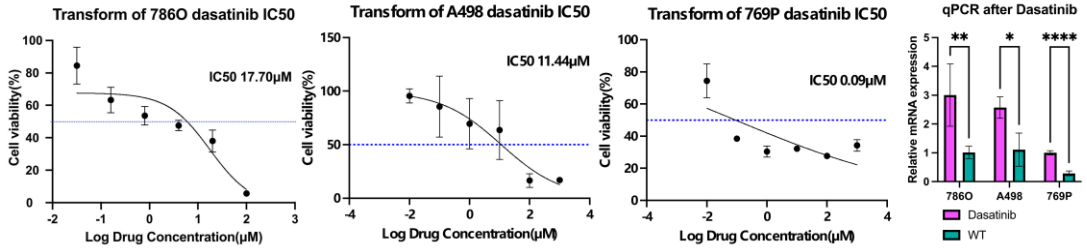

Figure S16. Dasatinib could significantly decrease NPR3 mRNA in 786-O, A-498, and 769-P cells. *qPCR, quantitative real-time polymerase chain reaction; WT, Wild Type; *p < 0.05, **p < 0.01, ***p < 0.001.*

Table S1 | 33 tumor types from TCGA and their abbreviation.

Tumor	Abbreviation
ACC	Adrenocortical carcinoma
BLCA	Bladder Urothelial Carcinoma
BRCA	Breast invasive carcinoma
CESC	Cervical squamous cell carcinoma and endocervical adenocarcinoma
CHOL	Cholangiocarcinoma
COAD	Colon adenocarcinoma
DLBC	Lymphoid Neoplasm Diffuse Large B-cell Lymphoma
ESCA	Esophageal carcinoma
GBM	Glioblastoma multiforme
HNSC	Head and Neck squamous cell carcinoma
KICH	Kidney Chromophobe
KIRC	Kidney renal clear cell carcinoma
KIRP	Kidney renal papillary cell carcinoma
LAML	Acute Myeloid Leukemia
LGG	Brain Lower Grade Glioma
LIHC	Liver hepatocellular carcinoma
LUAD	Lung adenocarcinoma
LUSC	Lung squamous cell carcinoma
MESO	Mesothelioma
OV	Ovarian serous cystadenocarcinoma
PAAD	Pancreatic adenocarcinoma
PCPG	Pheochromocytoma and Paraganglioma
PRAD	Prostate adenocarcinoma
READ	Rectum adenocarcinoma
SARC	Sarcoma
SKCM	Skin Cutaneous Melanoma
STAD	Stomach adenocarcinoma
TGCT	Testicular Germ Cell Tumors
THCA	Thyroid carcinoma
THYM	Thymoma
UCEC	Uterine Corpus Endometrial Carcinoma
UCS	Uterine Carcinosarcoma
UVM	Uveal Melanoma

Table S2 | TIDE analysis.

Cohort	Cancer	Subtype	CTL Correlation	T Dysfunction	Risk	Risk adjusted	Count
E-MTAB-179	Brain	Neuroblastoma	-0.01	1.177	-1.662	-1.536	389
GSE12417_GPL570	Leukemia	AML	-0.19	0.916	1.309	0.444	79
TCGA	Melanoma	Metastatic	-0.07	0.037	0.522	0.09	317
METABRIC	Breast	TN	-0.15	-1.636	0.751	0.503	233
TCGA	Endometrial		-0.048	-2.197	1.976	1.931	541

TCGA, The Cancer Genome Atlas; AML, Acute Myeloid Leukemia; TN, Triple Negative.